Energy transfer between Ce^{3+} and Sm^{3+} in Zn_2GeO_4 phosphor with the native defects for light-emitting diodes

Yushuang Qi (齐玉双)[1], Lei Zhao (赵 磊)[2], Wenjuan Bian (边文娟)[1], Xue Yu (余 雪)[1,3,*], Xuhui Xu (徐旭辉)[1,3], and Jianbei Qiu (邱建备)[1,3]

[1]*College of Materials Science and Engineering, Kunming University of Science and Technology, Kunming 650093, China*

[2]*Department of Physics and Information Technology, Baoji University of Arts and Sciences, Baoji 721016, China*

[3]*Key Laboratory of Advanced Materials of Yunnan Province, Kunming 650093, China*

**Corresponding author: yuyu6593@126.com*

Received April 6, 2017; accepted May 18, 2017; posted online June 12, 2017

A series of Ce^{3+}, Sm^{3+}-doped Zn_2GeO_4 phosphors are prepared by the solid-state reaction. A blue photoluminescence (PL) of Zn_2GeO_4 is observed as the recombination of the electrons trapped on $V_O^{\bullet}$ and $Zn_i^{\bullet}$ with holes trapped on V_{Ge} and V'_{Zn}. The energy transfer process between Ce^{3+} and Sm^{3+} is confirmed by the PL spectra and decay curves, and the emission colors can be adjusted from blue to orange–red. Furthermore, we verify unambiguously that the energy transfer from Ce^{3+} to Sm^{3+} occurs. Besides, Ce^{3+} ions can act as a bridge, possibly promoting the energy transfer from the Zn_2GeO_4 host matrix to Sm^{3+} ions.

OCIS codes: 160.0160, 230.0230, 300.0300.

doi: 10.3788/COL201715.081601.

White light-emitting diodes (w-LEDs) have drawn wide attention and extensive study for their low energy consumption, high brightness, long working lifetime, high efficiency, and environmentally friendly features[1–5]. Currently available commercial w-LEDs are fabricated by the combination of the blue-emitting LED chips and the yellow-emitting phosphors[6]. However, this approach suffers weaknesses, such as high color temperature, owing to the lack of a red light component. In order to improve the white performance, near ultraviolet (n-UV) (370–420 nm) LED chips coated with blue, green, and red-emitting phosphors is introduced. It provides an excellent color rendering index and low correlated color temperature. Thus, much attention has been concentrated on developing yellow–orange emitting phosphors, which provides more red emission components than yttrium aluminum garnet (YAG) Ce^{3+}[7]. Several oxynitrides have been developed for this purpose; however, the oxynitrides suffer from harsh preparation conditions, such as the carbothermal method or high-temperature nitrification at high pressure. Thus, it is important to explore novel efficient orange–yellow-emitting phosphors in an oxide host matrix through comparatively simple synthesis approaches for the practice application.

At present, numerous research efforts have been conducted to oxide phosphor with native defects. The native defect luminescent is observed in isolated d^{10} ion complexes, such as Zn_4O compounds, $Ca_3SnSi_2O_9$, GaN, and $BaMoO_4$[8–11]. There also exists strong evidence for the observation of photoluminescence (PL) from transition-metal oxides. Examples are β-Ga_2O_3, $SrZrO_3$, $SrTiO_3$, and $Sr_2V_2O_7$[12–15]. The studies attribute the radiative decay process to a distorted octahedral structure, self-trapped excitons, oxygen vacancies, surface states, and charge to transfer via intrinsic defects inside an oxygen octahedron[16]. Although there is no general consensus in the literature about the nature of the emission, it is a very interesting phenomenon to study these materials acting as the host matrix of LED phosphors, which could provide the energy transfer from the host matrix to activators.

Recently, there is some research focused on germanates as a host of optical materials. As a kind of garnet, germanates have a rich variety of material structure, the same as silicates. It can be expected that rare earth ions in the corresponding germanates' structure exhibit excellent luminescent characteristics. Li_2ZnGeO_4:Mn^{2+} exhibiting a green long persistent luminescence is reported by the Shang group[17], $CaZnGe_2O_6$:Mn^{2+} gives out a red luminescence as reported by the Che group, the Pan group explored a new type of $Zn_3Ga_2Ge_2O_{10}$:Cr^{3+} phosphor, which emits red at 698 nm[18], and the Xu group investigated $Na_2CaSn_2Ge_3O_{12}$:Sm^{3+} as a reddish-orange phosphor[19]. Among germanates, zinc germanate (Zn_2GeO_4) is an excellent candidate due to its reasonable conductivity and high stability. Zn_2GeO_4 has a rhombohedral structure, which is similar to Zn_2SiO_4, with Zn^{2+} ions at the tetrahedral sites and Ge at the octahedral sites, and it has a wide band gap of 4.68 eV[20]. Zn_2GeO_4 provides a potential application in field emission displays as a novel host matrix, and few literatures focus on its persistent luminescence properties[21]. Furthermore, Zn_2GeO_4 as a native defect phosphor is studied by the Qiu group[22]. Nevertheless, there is only limited study on the PL of Zn_2GeO_4, and no attempts have been made for energy transfer from the host to activators. In this work, we perform research on Ce^{3+},

Sm^{3+}-doped Zn_2GeO_4 phosphor, which emits a tunable color due to the effective energy transfer from the host to the activators. The PL properties of the Zn_2GeO_4 host matrix, Ce^{3+}, Sm^{3+} single, and co-doped samples are studied. The energy transfer process between Ce^{3+} and Sm^{3+} is investigated in detail.

The Zn_2GeO_4; $Zn_{1.99}GeO_4$:$0.01Sm^{3+}$; $Zn_{1.96}GeO_4$:$0.04Ce^{3+}$; $Zn_{1.99-x}GeO_4$:xCe^{3+}, $0.01Sm^{3+}$ ($x = 0.00$, 0.01, 0.02, 0.03, 0.04, and 0.05), and $Zn_{1.96-y}GeO_4$:$0.04Ce^{3+}$, ySm^{3+} ($y = 0.005$, 0.01, 0.03, 0.05, 0.07, and 0.09) samples are synthesized by the high-temperature solid-state reaction. As raw materials, ZnO (99.99%), GeO_2 (99.999%), Sm_2O_3 (99.99%), and CeO_2 (99.99%) are stoichiometrically weighted out. H_3BO_3 at 5% is employed as flux. After the ingredients are thoroughly mixed and ground in an agate mortar, the mixtures are placed into an alumina crucible. This crucible is heated at 1000°C for 12 h under air atmosphere and slowly cooled to room temperature. The phases of the obtained samples are identified by X-ray powder diffraction (XRD) with Cu Kα [$\lambda = 0.15418$ nm radiation at a scanning step of 0.02° in the 2θ range from 10° to 60°, operated at 36 kV and 30 mA (Rigaku Model D/max-2200)]. The PL and PL excitation (PLE) spectra are measured with a HITACHI F-7000 fluorescence spectrophotometer. The decay curves are recorded on an Edinburgh instruments FLS920 spectrometer. X-ray photoelectron spectra (XPS) are obtained using a PHI5000 Versaprobe-II; the spectrophotometer is American Standard Test Method (ASTM) calibrated and operated under a vacuum ($<4 \times 10^{-8}$ Pa). As the primary excitation source, non-monochromatic Mg Kα (400 W, 1253.6 eV) radiation is used at an angle of 0°C relative to the sample's surface normal.

The purity of all the prepared samples is systematically checked by XRD. Figure 1(a) shows the typical XRD patterns of Sm^{3+} and Ce^{3+}-doped Zn_2GeO_4 samples. All the diffraction peaks detected can be indexed to the pure phase of Zn_2GeO_4 (JCDPS No.11-0687). No obvious shifting of peaks or second phase is observed at the current doping level, indicating that Sm^{3+} and Ce^{3+} ions are completely dissolved in the Zn_2GeO_4 host matrix. Based on the effective ionic radii[23], Sm^{3+} ($r = 0.0958$ nm, CN = 6) and Ce^{3+} ($r = 0.095$ nm, CN = 6) ions are proposed to occupy the Zn^{2+} ($r = 0.074$ nm, CN = 6) sites rather than Ge^{4+} ($r = 0.053$ nm, CN = 6) sites, due to the fact that the sites of Ge^{4+} are too small for Ce^{3+} or Sm^{3+} to occupy. Due to the nonequivalent substitution, an excess of a positive charge in the lattice must be compensated. Two Ce^{3+} ions replace three Zn^{2+} ions to balance the charge of the phosphor, which create two positive defects and one negative defect. As the hole traps, Zn vacancies (V''_{Zn}) are formed by

$$2Ce^{3+} \xrightarrow{3Zn^{2+}} 2Ce^{\bullet}_{Zn} + V''_{Zn},$$

$$2Sm^{3+} \xrightarrow{3Zn^{2+}} 2Sm^{\bullet}_{Zn} + V''_{Zn}.$$

Figure 1(b) shows the XPS analyses of Zn^{2+} and Ge^{4+} when Ce^{3+} ions are doped in the phosphors. It indicates the presence of a relatively large amount of Zn, Ge, O, and Ce. In particular, the XPS of $Zn_{1.96}GeO_4$:$0.04Ce^{3+}$ is employed to elucidate the chemical state of Ce^{3+} ions. The enlargement of Fig. 1(b) shown in the inset can be well fitted with a distribution of a peak centered at 885.4 eV, which is attributed to Ce^{3+} ions.

Figure 2 shows the PLE and PL spectra of Zn_2GeO_4, Sm^{3+}, Ce^{3+} single-doped, and co-doped Zn_2GeO_4 samples at room temperature, respectively. As shown in Fig. 2(a), a broadband with a maximum at 446 nm is observed in the Zn_2GeO_4 host matrix, while an evidently symmetric band located around 267 nm is detected when the emission of 446 nm is monitored. The bluish PL of Zn_2GeO_4 derives from the recombination of the donor–acceptor, as discussed in a previous report[19]. That is, the electrons trapped on $V_O^{\bullet}$ and $Zn_i^{\bullet}$ are recombined with holes trapped on V_{Ge} and V'_{Zn} directly or through the conduction band. Figure 2(b) presents the PLE and PL spectra of Sm^{3+}-doped Zn_2GeO_4. It is found that Sm^{3+}-doped Zn_2GeO_4 exhibits similar PL properties as the Zn_2GeO_4

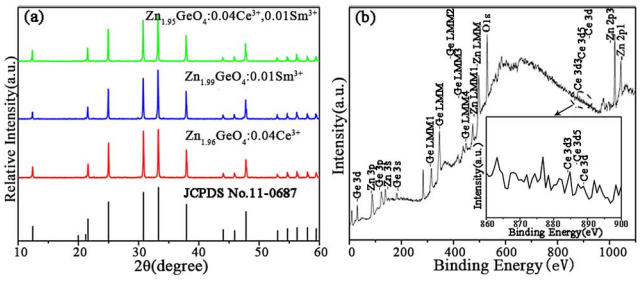

Fig. 1. (a) XRD patterns of $Zn_{1.99}GeO_4$:$0.01Sm^{3+}$, $Zn_{1.96}GeO_4$:$0.04Ce^{3+}$, $Zn_{1.95}GeO_4$:$0.04Ce^{3+}$, $0.01Sm^{3+}$, and the JCPDS card of Zn_2GeO_4 (No.11-0687), (b) XPS of $Zn_{1.96}GeO_4$:$0.04Ce^{3+}$, and the inset is the enlargement of the XPS spectrum from 860 to 900 eV.

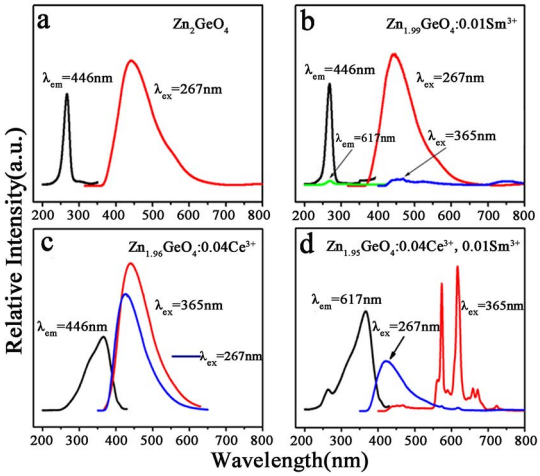

Fig. 2. (a) PLE and PL spectra of Zn_2GeO_4, (b) $Zn_{1.99}GeO_4$:$0.01Sm^{3+}$, (c) $Zn_{1.96}GeO_4$:$0.04Ce^{3+}$, and (d) $Zn_{1.95}GeO_4$:$0.04Ce^{3+}$, $0.01Sm^{3+}$ samples, respectively.

host matrix under the excitation at 267 nm. The characteristic emission of Sm^{3+} is not obvious with the excitation of 267 nm, indicating that the energy transfer between the Zn_2GeO_4 host matrix and Sm^{3+} is not effective. When monitoring the emission at 617 nm, a weak peak located at 267 nm is detected in the PLE spectrum. Both the PL of the host and Sm^{3+} are not observed under the excitation of 365 nm, indicating that both the host and Sm^{3+} ions could not be excited effectively in this host matrix. As shown in Fig. 2(c), the emission spectrum of Zn_2GeO_4:Ce^{3+} under the excitation of 267 nm is recorded, and the emission band located at 425 nm is observed, which is similar to the spectrum of the Zn_2GeO_4 sample. The PLE spectra of Zn_2GeO_4:Ce^{3+} exhibits a broadband at 200–450 nm with a maximum at 365 nm that is monitored at the emission of 446 nm, which exhibits asymmetry to some extent. However, consider the fact that the Zn_2GeO_4 could be excited under 267 nm, as discussed above. Therefore, the emission located at 425 nm in Zn_2GeO_4:Ce^{3+} originated from both the Zn_2GeO_4 host and Ce^{3+} ions. Besides, an intense blue emission in the range of 370–650 nm with the maximum peak located at 446 nm is detected under the excitation of 365 nm, which could be ascribed to the transitions of Ce^{3+} ions (5d → 4f). Therefore, it is safe to say that the Ce^{3+} ions could be excited by the energy aborted by the host matrix as a luminescent center. The PL spectrum of Zn_2GeO_4:Ce^{3+}, Sm^{3+} under the excitation at 267 nm is shown in Fig. 2(d) (blue line). It exhibits an obvious wide peak at 446 nm and two obscure spikes at 567 and 617 nm, ascribed to Sm^{3+} ions ($^4G_{5/2} \rightarrow {}^6H_{7/2}$, $^4G_{5/2} \rightarrow {}^6H_{5/2}$), respectively[24]. The PLE spectrum of Zn_2GeO_4:Ce^{3+}, Sm^{3+} is obviously different from that of Zn_2GeO_4:Sm^{3+} when the emission of 617 nm is monitored. The PLE spectrum of Zn_2GeO_4:Ce^{3+}, Sm^{3+}, consists of two bands located at 267 and 365 nm, which is ascribed to the characteristic excitation of the host matrix and Ce^{3+} ions, respectively, as discussed above. Therefore, Ce^{3+} acting as a bridge, conspicuously promotes the energy transfer from the host matrix Zn_2GeO_4 to Sm^{3+}, for Sm^{3+} ions exhibiting an insignificant intensity under the excitation of 267 nm. Besides, it is found that the emission of Ce^{3+} is almost insignificant, verifying that Sm^{3+} could be excited efficiently by the characteristic excitation transition of Ce^{3+} (365 nm). Thus, the energy transfer between Ce^{3+} to Sm^{3+} could be expected.

According to Dexter's theory[25], an efficient energy transfer requires a partial overlap between the excitation spectrum of the activator and the emission spectrum of the sensitizer. Figure 3 depicts the PLE of Zn_2GeO_4:Sm^{3+} (black) and the PL of Zn_2GeO_4:Ce^{3+} (red). The characteristics the PLE spectrum of Sm^{3+} exhibits the broad band absorption in the range of 200-430 nm, while the emission of Ce^{3+} ions, located at the 350–650 nm range, is attributed to the 5d → 4f transition[26]. The spectral overlap of the Sm^{3+} excitation and Ce^{3+} emission indicates that the energy transfer process from Ce^{3+} to Sm^{3+} occurs.

To further demonstrate the energy transfer from Ce^{3+} to Sm^{3+}, the PL spectra of $Zn_{1.99-x}GeO_4$:xCe^{3+}, $0.01Sm^{3+}$ (x = 0.00, 0.01, 0.02, 0.03, 0.04, and 0.05) are shown in Fig. 4. The emission intensities of Sm^{3+} increase remarkably with an increasing concentration of Ce^{3+} and reaches the maximum at $x = 0.04$; meanwhile, the emission intensity of Ce^{3+} at 446 nm is observed as almost insignificant. The characteristic emissions of Ce^{3+} are not observed, which suggests the effective energy transfer.

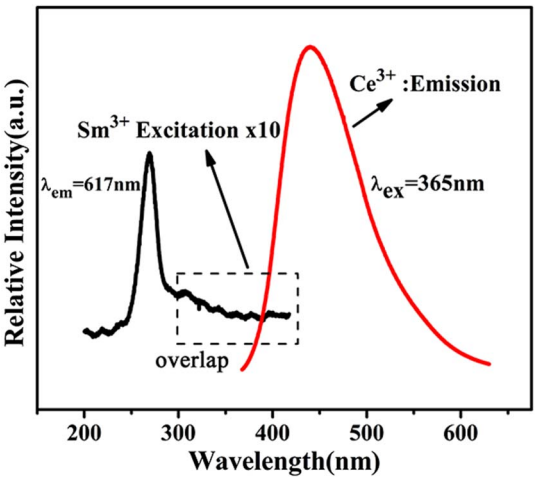

Fig. 3. (Color online) PLE spectrum of $Zn_{1.99}GeO_4$:$0.01Sm^{3+}$ (black) and PL spectrum of $Zn_{1.96}GeO_4$:$0.04Ce^{3+}$ (red).

In order to illustrate the energy transfer from Ce^{3+} and Sm^{3+}, the decay curves of $Zn_{1.96-y}GeO_4$:$0.04Ce^{3+}$, ySm^{3+} (y = 0.00, 0.005, 0.03, and 0.07) are measured, as shown in Fig. 5 (λ_{ex} = 365 nm, λ_{em} = 446 nm). It is found that all of the decay curves can be well fitted by the second-order exponential decay mode as the following equation[2]:

$$I = A_1 \exp(-t/\tau_1) + A_2 \exp(-t/\tau_2), \quad (1)$$

where I is the luminescence intensity, A_1 and A_2 are fitting parameters, t is the time, τ_1 and τ_2 are rapid and slow lifetimes for exponential components, respectively. The values of A_1, A_2, τ_1, and τ_2 are obtained, as shown in Table 1. Based on these parameters, the average decay time τ of Ce^{3+} can be calculated by the following equation[27]:

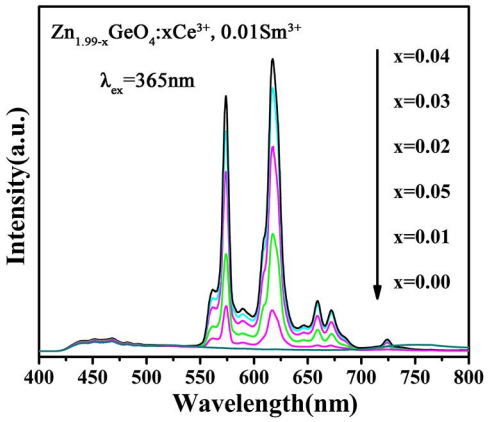

Fig. 4. PL spectra of $Zn_{1.99-x}GeO_4$:xCe^{3+}, $0.01Sm^{3+}$ (x = 0.00, 0.01, 0.02, 0.03, 0.04, and 0.05) samples.

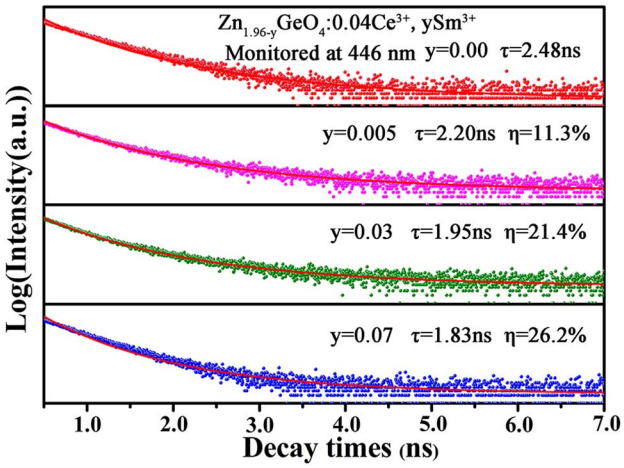

Fig. 5. Decay curves of $Zn_{1.96-y}GeO_4$:$0.04Ce^{3+}$, ySm^{3+} ($y = 0.00$, 0.005, 0.03, and 0.07) monitored the 446 nm emission under 365 nm excitation.

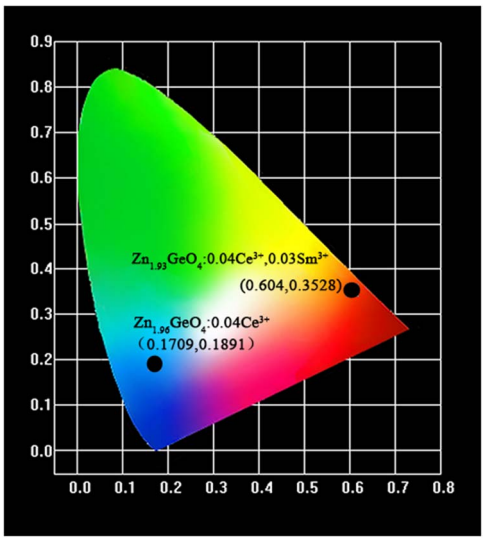

Fig. 6. CIE chromaticity diagram of $Zn_{1.96}GeO_4$:$0.04Ce^{3+}$ and $Zn_{1.93}GeO_4$:$0.04Ce^{3+}$, $0.03Sm^{3+}$ phosphors.

Table 1. Decay Kinetics for $Zn_{1.96-y}GeO_4$:$0.04Ce^{3+}$, ySm^{3+} ($y = 0.00$, 0.005, 0.03, and 0.07) Phosphors

τ_1 (ns)	A_1	τ_2 (ns)	A_2
1.4559	1142.543	13.2079	11.988
1.2594	1178.256	13.1723	9.651
1.2763	1147.682	11.5937	8.7932
1.422	1243.268	11.2764	9.143

$$\tau = \frac{A_1\tau_1^2 + A_2\tau_2^2}{A_1\tau_1 + A_2\tau_2}, \tag{2}$$

As shown in Fig. 5, the average decay times (τ) are determined to be 2.48, 2.20, 1.95, and 1.83 ns for $Zn_{1.96-y}GeO_4$:$0.04Ce^{3+}$, ySm^{3+}, $y = 0.00$, 0.005, 0.03, and 0.07, respectively. The decay time of Ce^{3+} decreases with the increased concentration of Sm^{3+}, which strongly confirms the existence of the energy transfer process from Ce^{3+} to Sm^{3+} in the Zn_2GeO_4 host.

The efficiency of the energy transfer from Ce^{3+} to Sm^{3+} can be estimated according to the following equation:

$$\eta = 1 - \tau_s/\tau_{s0}, \tag{3}$$

where η means the energy transfer efficiency, τ_s and τ_{s0} are on behalf of the lifetimes of Ce^{3+} in the absence and the presence of Sm^{3+}, respectively. As depicted in the inset of Fig. 5, the efficiency of the energy transfer ascends gradually from 11.3% to 26.2% with the increment of the concentration of Sm^{3+}.

The CIE chromaticity diagram of Zn_2GeO_4:Ce^{3+} and $Zn_{1.93}GeO_4$:$0.04Ce^{3+}$, $0.03Sm^{3+}$ phosphors under 365 nm are measured and presented in Fig. 6. The CIE coordinates shifted from (0.1709, 0.1891) to (0.604, 0.3528) in $Zn_{1.96}GeO_4$:$0.04Ce^{3+}$ and $Zn_{1.93}GeO_4$:$0.04Ce^{3+}$, $0.03Sm^{3+}$ samples, which indicates that the emitting color of these samples changes from blue to red–orange, accordingly.

In general, it is known that if the energy transfer belongs to the exchange interaction, the critical distance between the sensitizer and activator should be shorter than 0.3–0.4 nm. The critical distance R_c for the energy transfer from Ce^{3+} to Sm^{3+} ions can be calculated through the concentration quenching method. According to the equation proposed by Blasse[28],

$$R_c = 2\left(\frac{3V}{4\pi X_c N}\right)^{1/3}, \tag{4}$$

where V is the volume of the unit cell, and N is the number of the center cations in the unit cell. The crystallographic data and the above calculation are given as follows: $V = 0.5632$ nm^3 and $N = 6$. X_c is the critical concentration (the total concentration of sensitizer of Ce^{3+} ions and activator ions of Sm^{3+}), where the emission of $Zn_{1.96-y}GeO_4$:$0.04Ce^{3+}$, ySm^{3+} phosphors reaches the maximum. Herein, $X_c = 0.07$ is the sum of Ce^{3+} concentration with 0.04 and the critical concentration of Sm^{3+} with 0.03. Accordingly, the critical energy transfer distance for Ce^{3+} and Sm^{3+} in the Zn_2GeO_4 host is calculated to be 1.3682 nm. The value is much larger than 0.4 nm, which shows that the electric multi-polar interaction rather than the exchange interaction is responsible for the energy transfer from Ce^{3+} to Sm^{3+} in the Zn_2GeO_4 host.

According to Dexter's energy transfer formula of multipolar interaction and Reisfeld's approximation[29], $(\eta_{s0}/\eta_s) \propto C^{n/3}$, where η_{s0} and η_s are the luminescence quantum efficiencies of the sensitizer (Ce^{3+}) in the absence and presence of the activator (Sm^{3+}), respectively. The relation $(\eta_{s0}/\eta_s) \propto C^{n/3}$ can be obtained, and the value η_{s0}/η_s is an approximation calculated by the I_{s0}/I_s[30]. C is the sum of the content of Ce^{3+} and Sm^{3+}.

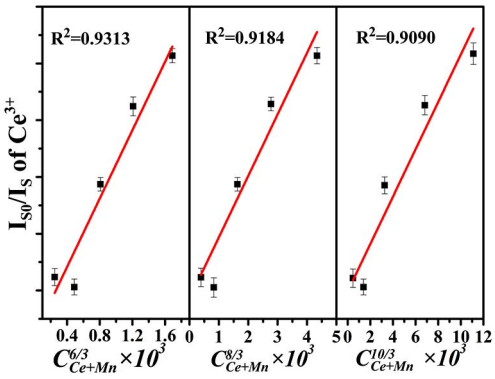

Fig. 7. Dependence of I_{s0}/I_s of Ce^{3+} on $C^{6/3}$, $C^{8/3}$, and $C^{10/3}$.

$n = 6$, 8, and 10, corresponding to the dipole–dipole, dipole–quadrupole, and quadrupole–quadrupole interactions. The relations between I_{s0}/I_s and $C^{n/3}$ when $n = 6$, 8, 10 are illustrated in Fig. 7. It is obvious that $n = 6$ fits well with the liner relationship, illustrating that the energy transfer from Ce^{3+} to Sm^{3+} is realized mainly through the dipole–dipole interaction. The error bars in Fig. 7 represent the standard deviation, and their values are less than 0.3.

In conclusion, Ce^{3+}, Sm^{3+}-doped Zn_2GeO_4 phosphors are prepared by a traditional solid-state reaction in this work. The efficient energy transfer process between Ce^{3+} and Sm^{3+} is investigated by the decay curves. The emission color changes from blue in Zn_2GeO_4:Ce^{3+} to orange–red in Zn_2GeO_4:Ce^{3+}, Sm^{3+} via the efficient energy transfer from Ce^{3+} to Sm^{3+}. Besides, Ce^{3+} acting as a bridge, can promote the energy transfer from Zn_2GeO_4 to Sm^{3+} inconspicuously. The results indicate that Zn_2GeO_4:Ce^{3+}, Sm^{3+} phosphor provides a potential application as an efficient orange–red phosphor for LEDs.

This work was supported by the National Nature Science Foundation of China (Nos. 61565009 and 61308091), the Young Talents Support Program of Faculty of Materials Science and Engineering, Kunming University of Science and Technology (No. 14078342), and the Postdoctoral Science Foundation of China (No. 2013M540720).

References

1. D. Q. Chen, Y. Zhou, W. Xu, J. S. Zhong, Z. G. Ji, and W. D. Xiang, J. Mater. Chem. C **4**, 1704 (2016).
2. H. Li, Y. Zhang, X. Chen, C. Wu, J. Guo, Z. Gao, and H. Chen, Chin. Opt. Lett. **13**, 080605 (2015).
3. Z. Li, H. Wang, B. Yu, X. Ding, and Y. Tang, Chin. Opt. Lett. **15**, 042301 (2017).
4. S. D. Yu, Z. T. Li, G. W. Liang, Y. Tang, B. H. Yu, and K. H. Chen, Photon. Res. **4**, 140 (2016).
5. Y. Chen, S. Wen, and P. Song, Chin. Opt. Lett. **13**, 032302 (2015).
6. Y. Chen, F. J. Pan, M. Wang, X. J. Zhang, J. Wang, M. M. Wu, and C. X. Wang, J. Mater. Chem. C **4**, 2367 (2016).
7. Q. Wang, D. Deng, Y. Hua, L. Huang, H. Wang, S. Zhao, G. Jia, C. Li, and S. Xu, J. Lumin. **132**, 434 (2012).
8. S. Kumar, C. Tessarek, S. Christiansen, and R. Singh, J. Alloy. Comp. **587**, 812 (2014).
9. G. F. Yang, P. Chen, S. M. Gao, G. Q. Chen, R. Zhang, and Y. D. Zheng, Photon. Res. **4**, 17 (2016).
10. X. Xu, Y. Wang, W. Zeng, Y. Gong, and B. Liu, J. Am. Ceram. Soc. **94**, 3632 (2011).
11. Y. F. Liu, L. L. Xia, Y. N. Lu, S. H. Dai, M. Takeguchi, H. M. Hong, and Z. G. Pan, J. Colloid Interf. Sci. **381**, 24 (2012).
12. M. Higashiwaki, K. Sasaki, A. Kuramata, T. Masui, and S. Yamakoshi, Appl. Phys. Lett. **100**, 013504 (2012).
13. Z. Guo, L. Zhu, J. Zhou, and Z. Sun, J. Mater. Chem. C **3**, 4081 (2015).
14. V. B. Taxak and S. P. Khatkar, J. Fluoresc. **22**, 891 (2012).
15. Z. Zhou, N. Wang, N. Zhou, Z. He, S. Liu, Y. Liu, Z. Tian, Z. Mao, and H. T. Hintzen, J. Phys. D. Appl. Phys. **46**, 035 (2013).
16. W. F. Zhang, J. W. Tang, and J. H. Ye, Chem. Phys. Lett. **418**, 174 (2006).
17. Y. Jin, Y. Hu, H. Duan, L. Chen, and X. Wang, RSC. Adv. **4**, 11360 (2014).
18. J. Li, J. Shi, J. Shen, H. Man, M. Wang, and H. Zhang, Nano. Lett. **7**, 138 (2015).
19. J. Xu, Z. Ju, X. Gao, Y. An, X. Tang, and W. Liu, Inorg. Chem. **52**, 13875 (2013).
20. G. Anoop, K. Mini Krishna, K. Rajeev Kumar, and M. K. Jayaraj, J. Electrochem. Soc. **155**, J270 (2008).
21. M. Wan, Y. Wang, X. Wang, H. Zhao, and Z. Hu, Opt. Mater. **36**, 650 (2014).
22. H. L. He, Y. H. Zhang, Q. W. Pan, G. B. Wu, G. P. Dong, and J. R. Qiu, J. Mater. Chem. C **3**, 5419 (2015).
23. Y. Q. Jia, J. Solid. Chem. **95**, 184 (1991).
24. X. Min, Z. Huang, M. Fang, Y. G. Liu, C. Tang, and X. Wu, Inorg. Chem. **53**, 6060 (2014).
25. M. Shang, G. Li, D. Yang, X. Kang, C. Peng, and J. Lin, Dalton Trans. **41**, 8861 (2012).
26. Z. Ci, Q. Sun, M. Sun, X. Jiang, S. Qin, and Y. Wang, J. Mater. Chem. C **16**, 11597 (2014).
27. L. L. Han, Y. H. Wang, L. Zhao, J. Zhang, Y. Z. Wang, and Y. Tao, Opt. Mater. **36**, 1203 (2014).
28. Y. Cui, S. Zhao, Z. Liang, M. Han, and Z. Xu, J. Alloy. Comp. **593**, 30 (2014).
29. K. Li, Y. Zhang, X. J. Li, M. M. Shang, H. Z. Lian, and J. Lin, Dalton. Trans. **44**, 4683 (2015).
30. D. L. Dexter and J. A. Schulman, J. Chem. Phys. **22**, 1063 (1954).